Dyes and Pigments 171 (2019) 107696

Contents lists available at ScienceDirect

Dyes and Pigments

journal homepage: www.elsevier.com/locate/dyepig

A PHBA-functionalized organic-inorganic hybrid polyoxometalate as a luminescent probe for selectively sensing chromium and calcium in aqueous solution

Hechen Wu, Hanhan Chen, Minghui Fu, Rui Li, Pengtao Ma*, Jingping Wang, Jingyang Niu**

Henan Key Laboratory of Polyoxometalate Chemistry, College of Chemistry and Chemical Engineering, Henan University, Kaifeng, Henan, 475004, China

ARTICLE INFO

Keywords:
Polyoxometalates
Luminescent sensor
Cr^{3+} ion
Ca^{2+} ion

ABSTRACT

Detection of trace metal ions in drinking as well as irrigation water is crucial in understanding their roles among living humans and animals. Herein, an organic PHBA-functionalized polyoxometalate (POM) derivative $[N(CH_3)_4]_3K_2Eu(PHBA)(H_2O)_2(\alpha\text{-}PW_{11}O_{39})]\cdot 7H_2O$ (**1**) (PHBA = *p*-hydroxybenzoic acid) was successfully synthesized which acts as a luminescent probe for selective sensing of chromium and calcium in aqueous solution. The aqueous solution photoluminescence properties of **1** were carefully investigated, indicating PHBA ligand can sensitize the luminescence of Eu^{3+} ion in **1**. The time-resolved emission spectroscopy was also performed to authenticate the energy transfer from π-π^* transition of PHBA group to Eu^{3+} ion. The sensing properties of **1** were performed on Cd^{2+}, Cr^{3+}, Ba^{2+}, K^+, Li^+, Pb^{2+}, Zn^{2+}, Al^{3+}, Ag^+, Hg^{2+}, Co^{2+}, Sr^{2+}, Ca^{2+}, Na^+, Mg^{2+} ions in aqueous solution, and the photoluminescence intensity for Cr^{3+} ion display a quenching phenomenon, whereas, Ca^{2+} ion displays an enhancement signal in their photophysical behavior. The detection limits for detecting Cr^{3+} and Ca^{2+} ion were 1.423 μM and 0.676 mM, respectively. In the detection process of Cr^{3+} ion, the values of quenching rate constant (K_q) were varied from 4.34×10^6 L $(mol\ s)^{-1}$ to 4.29×10^9 L $(mol\ s)^{-1}$, which were lower than the value of the maximum scatter collision quenching constant (2.0×10^{10} L $(mol\ s)^{-1}$). The results reveal that the quenching mechanism between **1** and Cr^{3+} ion can be attributed to dynamic collision quenching mechanism. Furthermore, the active sites for sensing Cr^{3+} and Ca^{2+} ions also have been investigated, determining the different interaction mechanisms exist in detection of Cr^{3+} and Ca^{2+} ions in solution.

1. Introduction

Recently, heavy metal pollution has become a more and more severe challenge in all over the world, especially for drinking and irrigation water, which is indeed a serious concern as it leads to a series of foreseeable and unforeseen diseases that threaten the safety of human life in the contemporary society [1–5]. Trivalent chromium (Cr^{3+}) are known to be harmless and necessary species in many biological processes as well as used frequently in industrial process, while excessive Cr^{3+} concentration can coupled with DNA in the human bodies, resulting in mutations or malignant cells and increasing the risk of diabetes and cardiovascular diseases related to other complications [6–11]. Calcium is the essential element for the formation of basic skeleton in human and other animal bodies, the lack of calcium element can lead to a series of severe diseases, while the excess of calcium element also could cause stone problems in living body [12]. Therefore, selective and sensitive detection of metal ions in solution is an urgent issue and of great importance to human security and environmental protection, and the metal ions to a certain degree play a crucial role in a variety of vital cell functions [13]. Up to now, the selective detection of metal ions, including UV–vis absorption, atomic absorption spectrophotometry, fluorescence detection, inductively coupled plasma emission spectroscopy, and voltammetry, have been acquiring a burgeoning interest [14–17]. Among the dazzling detection technologies, the fluorescence detection has been becoming a feasible operation as a consequence of the high selectivity, convenience, rapid response, facile operation and so forth [18–22]. In the traditional operations, organic fluorescent molecules were supposed as excellent fluorescence probes due to their desirable luminescence behaviors and active sites. In the organic molecules, the Lewis basic sites, such as pyridyl nitrogen, amide groups and OH components, have been affirmed to recognize and trace neutral as well as ionic species [23–25]. The interaction mechanism

* Corresponding author.
** Corresponding author.
E-mail addresses: mpt@henu.edu.cn (P. Ma), jyniu@henu.edu.cn (J. Niu).

https://doi.org/10.1016/j.dyepig.2019.107696
Received 11 May 2019; Received in revised form 26 June 2019; Accepted 2 July 2019
Available online 03 July 2019
0143-7208/

between Lewis basic sites and metal ions (Lewis acid) can be regulated through their varieties and concentrations [26–30].

Polyoxometalates (POMs), as a series of anionic metal oxide clusters of Mo, W, V, Nb and Ta, are quite promising in many fields, such as magnetic, catalysis, optical and electrical materials due to their abundant structure and distinct properties [31–37]. The cooperation of lanthanide ion (Ln^{3+}) and POMs fragments (Ln-POM) have been widely explored in a good deal of potential applications ranging from single molecular magnetic, single ion magnetic, optical materials, high-nuclear clusters to Lewis catalysis [38–40]. Interestingly, the Ln-POM derivatives can also be regarded as one kind of potential fluorescence sensor because of their satisfactory luminescence behaviors derived from f-f transitions of Ln^{3+} ions, such as sharp emissions, long lifetime, high color purity, etc [41,42]. Till now, several inorganic POMs incorporating Ln^{3+} centers have been shown to act as efficient luminescent probes [43–47], while relatively rare efforts were done to sense heavy metal ions. For example, Mialane and coworkers reported one EuW10@UiO-67 composite as chemical probe for sensing Na^+, K^+, Ni^{2+}, Cr^{3+}, Cu^{2+}, Al^{3+}, Mn^{2+}, and Fe^{3+} ions, showing a highly selective signal for Fe^{3+} ion in aqueous solutions [48]. The results reveal that the concentration limit for the detection is estimated to be 37 μM. Recently, Wang and coworkers prepared a series of Keggin compounds as bifunctional sensors to selectively sense Hg^{2+} ion in dimethyl sulfoxide (DMSO) solutions, and the detecting concentration of Hg^{2+} ion is 15 mM [49].

Herein, we successfully obtained one case of PHBA (PHBA = *p*-hydroxybenzoic acid, Scheme 1) functionalized Eu-POM ($[N(CH_3)_4]_3K_2Eu(PHBA)(H_2O)_2(\alpha\text{-}PW_{11}O_{39})]\cdot 7H_2O$, (**1**) as a new fluorescence sensor for detecting metal ions in aqueous solution. The reasons can be explained as: (a) in comparison with other Ln^{3+} ions, Eu^{3+} ion possess much higher inherent luminescence nature; (b) the excellent water solubility of POM may surmount the traditional bottleneck for detection of organic fluorescent molecules and increase the solubility of this sensor. Furthermore, the advantages of introducing organic PHBA into compound **1** are: (a) the organic PHBA ligand can efficiently absorb energy to sensitize emissions of Eu^{3+} ion via effective bond-through mechanism [41,50,51]; (b) the OH group from the PHBA serving as Lewis basic site can catch metal ions for the detection of heavy metal ions; (c) the carboxyl group from the PHBA was easy to bind f-metal ions for the formation of POM-based hybrids. Based on above facts, the composite of PHBA, Eu^{3+} ion and POM fragment has been well prepared and characterized by various physical and chemical technologies.

In this paper, overall fifteen metal ions (Cd^{2+}, Cr^{3+}, Ba^{2+}, K^+, Li^+, Pb^{2+}, Zn^{2+}, Al^{3+}, Ag^+, Hg^{2+}, Co^{2+}, Sr^{2+}, Ca^{2+}, Na^+, Mg^{2+}) have been tested in aqueous solution, and the results demonstrated that this sensor not only displays a high luminescence quenching effect upon several d-transition ions (e.g., Cr^{3+}, Co^{2+}, Ag^+), but also exhibits one luminescence enhanced phenomenon toward some metal ion (e.g., Ca^{2+}). As we know, considerable efforts have been performed on the detection of Ag^+, Mg^{2+}, Zn^{2+} and other ions [52–54], nevertheless, relatively rare documents were focused on the development of tracing and sensing of Cr^{3+} ions. The previous reports about detection of Cr^{3+} ions could lead to μM [55–57], or even to nM level, but only a few works based on POM derivatives were reported till now. Here, the designed sensor **1** is highly meaningful as it exhibits a very low detection limit until 1.423 μM level toward Cr^{3+} ion in aqueous solution. Furthermore, the photoluminescence of Eu^{3+} ion and energy transfer mechanism from PHBA to Eu^{3+} ion was systematically investigated by multifarious operations, respectively. Meanwhile, the exploration of interaction mechanisms between this POM-based probe and metal ions illustrate different interaction mechanisms prevailing in detection of Cr^{3+} and Ca^{2+} ions.

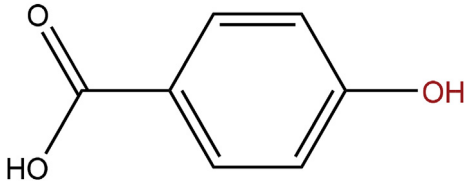

Scheme 1. The schematic of the ligand PHBA (PHBA = *p*-hydroxybenzoic acid).

2. Experimental details

2.1. Materials and methods

All chemicals were commercially purchased and used without any further purification. The precursor $K_{14}[P_2W_{19}O_{69}(H_2O)]\cdot 24H_2O$ was prepared according to a reported approach and confirmed by Fourier transform infrared (FTIR) spectrum [58]. C, H, and N elemental analyses were performed using an Elementar Vario EL cube CHNS analyzer. Powder X-ray diffraction (PXRD) data were collected on an X-ray powder diffractometer (Bruker, D8 Advance) using Cu Kα radiation (λ = 1.5418 Å) collected with the angular range (2θ) from 5° to 45° at room temperature. FTIR spectra (KBr disk) were performed using a Bruker VERTEX-70 spectrometer using KBr pellets in the region of 400–4000 cm^{-1}. The thermogravimetric analyses (TGA) cures were recorded from 30 °C to 800 °C with a heating rate of 10 °C min^{-1} in flowing N_2 atmosphere on a NETZSCH STA 449 F5 Jupiter thermal analyser. The Electrospray Ionization Mass Spectrometry (ESI-MS) spectrum measurements were performed on a Q EXACTIVE mass spectrometry in the negative ion mode and the collected data were analyzed using the Peak view 2.0 software. Photoluminescence emission spectra, photoluminescence excitation spectra, decay time curves and time-resolved emission spectroscopy were taken on an EDINBURGH FLS 980 fluorescence spectrophotometer equipped with a monochromated 325 W Xe-arc excitation source and a visible detector (Hamamatsu R928P). The single exponential function of decay time curve: $I(t) = Ae^{(-t/\tau)}$; where I(t) is the emission intensity at time t, A is the pre-exponential factor of lifetime τ [59].

2.2. Synthesis of *1*

$EuCl_3\cdot 6H_2O$ (0.228 g, 0.600 mmol) was dissolved into 30 mL deionized water in a beaker and stirred quickly until a clear solution appears, then the PHBA ligand (0.240 g, 0.200 mmol) and $K_{14}[P_2W_{19}O_{69}(H_2O)]\cdot 24H_2O$ precursor (2.120 g, 0.465 mmol) were added to the clear solution under stirring. The mixed solution stirred constantly to become clear. The pH value of above clear solution was regulated to 4.5 by 3 mol L^{-1} KOH solution under stirring. Finally, the resulting solution was heated at 80 °C for about 1.5 h, and then tetramethylammonium chloride (TMACl) (0.110 g, 1.000 mmol) was added and further stirred for 20 min. The resulting solution was cooled and filtered to evaporate at ambient temperature. The colorless block crystals were obtained after about 2 weeks. The obtained yield: 25.76% (0.530 g, based on $EuCl_3\cdot 6H_2O$). Selected FTIR (KBr pellets, cm^{-1}): 3050 (w), 1600 (m), 1520 (s), 1489 (s), 1414 (s), 1090 (s), 1051 (s), 955 (s), 886 (s), 825 (s) and 702 (m). Elemental analyses (%): Calcd, C, 6.56; H, 1.73; N, 1.23; Found, C, 6.78; H, 1.85; N, 1.22.

2.3. X-ray crystallography

A suitable good-quality sample of **1** was sealed in a capillary tube, and then the crystallographic data were corrected on a Bruker Apex II CCD diffractometer at room temperature using graphite-monochromated MoKα radiation (λ = 0.71073 Å). Empirical absorption corrections were carried out using a multi-scan absorption correction. All these structures were solved by direct methods and refined by full-matrix least squares on F^2 using the SHELXL-2018/1 program package [60,61]. During the solving and refinement process, all heavy atoms

were first located by full matrix least-squares refinements on F^2 and Fourier syntheses using the SHELXS-1997 program package, and which were further refined anisotropically. Most lattice water molecules were located by using a Fourier map, and the remaining lattice water molecules were determined by TGA results. The hydrogen atoms from the organic groups were placed in calculated positions and refined using a riding model. All hydrogen atoms on water molecules could not be well located from the electron density map. Crystallographic data for **1** with CCDC number of 1892872 can be obtained free from the Cambridge Crystallographic Data Center. Crystallographic data and structure refinements for **1** are listed in Table S1.

2.4. Luminescence sensing experiments

The crystal samples of **1** (0.087 g) was dispersed in a deionized aqueous solution (25 mL), and then the admixture is shaken on an oscillator for 10 min to a completed dissolved solution (1.0×10^{-3} mol/L); the solution was then used for the luminescence sensing measurements. The aqueous solutions of MCl_x (M = Cd^{2+}, Cr^{3+}, Ba^{2+}, K^+, Li^+, Pb^{2+}, Zn^{2+}, Al^{3+}, Ag^+, Hg^{2+}, Co^{2+}, Sr^{2+}, Ca^{2+}, Na^+, Mg^{2+}) were prepared for luminescence sensing measurements at the room temperature. Each MCl_x solution was initially going to be 1.0 mol/L, and the solution was diluted to continue the sensing experiments. For the luminescence measurements, 1.5 mL solution of **1** and 0.5 mL solution of MCl_x were together mixed in a quartz cube to run a luminescence test; each luminescence test was performed at the same conditions.

3. Results and discussion

3.1. FTIR, PXRD, TGA characteristics

The FTIR spectra of **1** and PHBA ligand were performed using KBr pellets on a Bruker VERTEX 70 IR spectrometer from 450 to 4000 cm^{-1} (Fig. S1). The strong peaks of FTIR spectra of **1** ranging from 700 cm^{-1} to 1100 cm^{-1} could be assigned to the high ν(P–O_a), ν(W–O_t), ν(W–O_b) and ν(W–O_c) vibrations bands of [α-$PW_{11}O_{39}$]$^{7-}$ subunits in **1** [42]. Compared to the FTIR spectrum of PHBA ligand, the FTIR spectrum of **1** display several peaks in the range of 1400–1600 cm^{-1}, (1414, 1489, 1520, and 1600 cm^{-1}) which can be attributed to the stretching vibrations of aromatic ring of PHBA ligand (1423, 1450, 1510, and 1597 cm^{-1}), and the blue shift may be attributed to the coordination effect between [$EuPW_{11}O_{39}$]$^{4-}$ unit and PHBA ligand. The above analyses provide the valid evidence that the existence of POM skeletons and organic group in **1**, are in good agreement with structural analyses from single-crystal X-ray diffraction (described in crystal structure section). As shown in Fig. S2, the experimental PXRD diagram of **1** have the similar patterns to the simulated diffraction patterns from the single crystal X-ray diffraction structural analysis of **1**, indicating the experimental samples are in good phase purity. Furthermore, the different pattern intensity between experimental and simulated PXRD patterns could be obviously observed, which may be due to the variations in preferred orientation of the experimental samples during the process of collection of the PXRD patterns. The TGA curve of **1** was collected under the N_2 atmosphere ranging from 30 °C to 800 °C. As shown in Fig. S3, the curve of **1** display two weight losses. The first step weigh loss of 3.74% from 30 to 160 °C, corresponds to the removal of seven lattice water (calcd. 3.68%). The second step weigh loss of 7.11% between 160 and 500 °C was assigned as the release of two coordinated water molecules and oxidation of three [$N(CH_3)_4$]$^+$ cations (calcd. 7.53%). The continued weigh loss in the range of 500–800 °C can be attributed to the oxidation of organic PHBA group and partial decomposition of POM skeleton [62,63].

3.2. Synthetic discussion

In the synthetic process, the final compound was obtained by the reaction of $EuCl_3$, PHBA ligand and $K_{14}[P_2W_{19}O_{69}(H_2O)]\cdot 24H_2O$ precursor in a suitable molar ratio. Parallel experiments show that the collection of target products depend on several factors: (a) the suitable pH environment. The parallel experiments were performed under the same condition except for pH value, which were set at 2.0, 2.5, 3.0, 3.5, 4.0, 4.5, 5.0, 5.5, 6.0, 6.5. The results show that the same product was obtained in the pH range of 4.0–4.5; (b) the effect of tetramethylammonium cations. The product was collected as tetramethylammonium salts from the resulting solution in the form of a crystalline solid. The experiment results indicate the final block crystals can not be obtained in the absence of the tetramethylammonium chloride; (c) the reaction temperature. The reaction temperature also affects the syntheses of products. The experiments have proved that the suitable reaction temperature from 70 °C to 80 °C can facilitate the syntheses of products.

3.3. Structure description of *1*

1 was successfully synthesized using a conventional aqueous method, and the single crystal diffraction analyses display that **1** crystallizes in the triclinic space group P-1. In detail, **1** comprises one [Eu(PHBA)$(H_2O)_2$(α-$PW_{11}O_{39}$)]$^{5-}$ polyanion (Fig. 1), two K^+ ions, three [$N(CH_3)_4$]$^+$ cations and seven lattice water molecules. In the polyanion of [Eu(PHBA)$(H_2O)_2$(α-$PW_{11}O_{39}$)]$^{5-}$, Eu^{3+} center belongs to eight-coordination configuration which is defined by four O atoms (O12, O14, O29, O30) provided by lacunary Keggin-type anion [α-$PW_{11}O_{39}$]$^{7-}$ with the Eu–O bond lengths being in the range of 2.325(3)–2.377(3) Å, two O atoms (O1W, O2W) occupied by coordinated water molecules with the Eu–O bond lengths ranging from 2.437(3) to 2.474(4) Å, and two O atoms (O40, O41) derived from carboxy group of PHBA ligand with the Eu–O bond lengths being between 2.465(3) and 2.519(3) Å, which are well consistent with the reported Eu–O distances [64]. As demonstrated in Fig. 2, the polyanion of **1** was orderly arranged through electrostatic interaction efforts. In addition, multiple O–H···O hydrogen bonds exist between the hydroxy of *p*-hydroxybenzoic ligand and water molecule (O8W) together with among the abundant water molecules with the O···O distances in the range of 2.64–2.84 Å within this matrix.

3.4. ESI-MS analysis

The ESI-MS is an efficient tool that affords a lot of reliable information of cluster molecule in solution [65]. Herein, the negative-ion ESI-MS analysis was used to study solution stability of **1** at room temperature. The single crystals of **1** were dissolved in water to obtain negative mode mass spectra of **1** (Fig. 3). The spectrum shows two peaks at *m/z* 741.5777 (simulated 741.5713) and 751.5926 (simulated 751.5336), attributed to the intact cluster [Eu($C_7H_5O_3$)(α-$PW_{11}O_{39}$)]$^{4-}$

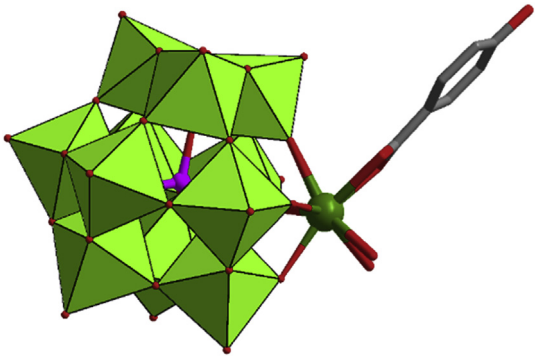

Fig. 1. The ball-and-stick/polyhedral representation of polyanion of **1**. Note that all H atoms were deleted for clarity. (color code: WO_6, bright green; W, bright green; P, pink; Eu, green; O, red; C, gray). (For interpretation of the references to color in this figure legend, the reader is referred to the Web version of this article.)

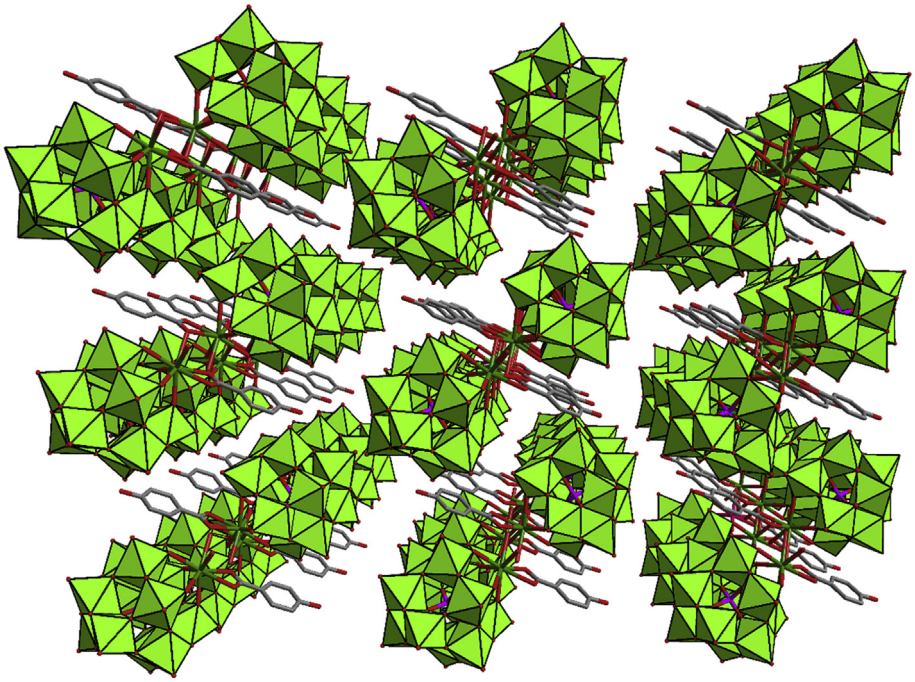

Fig. 2. The ball-and-stick/polyhedral representation of packing arrangement of polyanions for **1**. Note that all K^+ ions, $[N(CH_3)_4]^+$ cations, water molecules and H atoms were omitted for clarity.

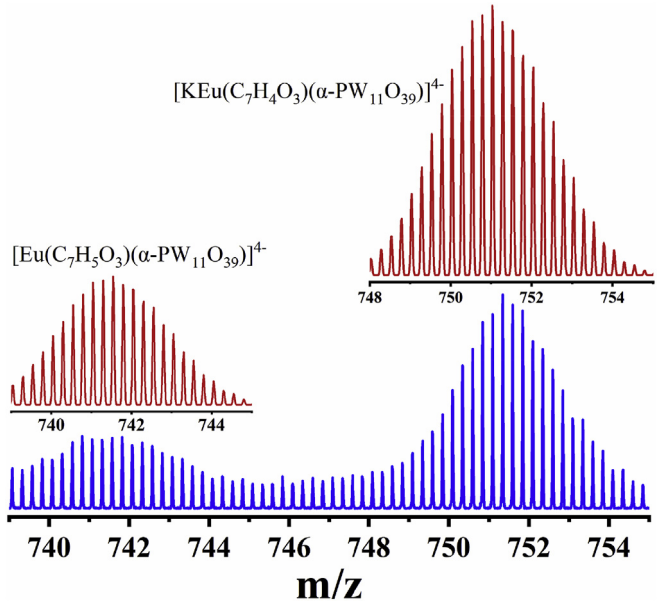

Fig. 3. ESI-MS spectra vesting in the complete polyanion for **1**. Note: simulated (red) and experimental (blue). (For interpretation of the references to color in this figure legend, the reader is referred to the Web version of this article.)

and $[KEu(C_7H_4O_3)(\alpha\text{-}PW_{11}O_{39})]^{4-}$ of compound **1**, respectively. The results clearly prove the stability of the complete polyanion of **1** in aqueous solution.

3.5. Photoluminescence properties

Up to now, the photoluminescence behaviors of Ln-POM derivatives have been systematically explored by previous works [66–68]. In the past few years, our group also have made a considerable contribution in this field [39,40,69–73]. According to the previous documents, the luminescence of Ln-POM complexes mainly originates from f-f electric-dipole transitions of Ln^{3+} ions, which is generally forbidden due to same parity 4f electronic configurations in Ln^{3+} ions. Therefore, the POM component could be seemed as sensitizer to some extent to break this dilemma, realizing the intense emitting emissions of Ln^{3+} ions in Ln-POMs, which have been proved through various physical-chemical tools [42,72]. However, the luminescence of Ln^{3+} ions aroused by organic chromophore groups has been not wide developed within Ln-POM molecules, and Boskovic and Zhou detailly investigated this mechanism in recent years, and the results show that the organic chromophore groups can provide a more efficient route for the sensitization of Ln^{3+} emitting centers [50,51,68].

Herein, the photoluminescence behaviors of **1** in aqueous solution were discussed. On the basis of the reported works, the photoluminescence excitation spectrum of **1** was recorded under emission at 619 nm. As shown in Fig. 4a, four excitation bands appeared at 330, 365, 382 and 395 nm in the excitation spectrum of **1**. The narrow peaks at 365, 382 and 395 nm could be attributed to the characteristic direct excitations of $^7F_0 \rightarrow {}^5D_4$, $^7F_0 \rightarrow {}^5G_2$, and $^7F_0 \rightarrow {}^5L_2$ f-f transitions of Eu^{3+} ion, respectively, and the broad band at 330 nm may be ascribed to the π-π* transition of PHBA group, indicating the organic PHBA ligand can absorb energy and subsequently transfer energy to sensitize the luminescence emission of Eu^{3+} ion. On the basic of above analyses, the photoluminescence emission spectrum of **1** was performed upon excitation at 330 nm (Fig. 4b), five characteristic emissions of Eu^{3+} ion at 582, 592, 619, 650 and 700 nm appeared in the emission spectrum, demonstrating the organic PHBA molecule facilitate the sensitization of Eu^{3+} ion. In detail, the five bands deactivate from the same excited level, $^5D_0$, to the ground quintet levels, ^7F_J (J = 0–4), of Eu^{3+} emitting center, respectively, which have been certified by the similar decay time layouts of different emissions (Fig. S4). It is worth noting that the most intense transition $^5D_0 \rightarrow {}^7F_2$ at 619 nm was mainly due to electric-dipole transitions. The broad emission band at 410 nm arise from π-π* transition of PHBA ligand, and it also proved that the presence of PHBA group within **1**.

To the best of our knowledge, the photoluminescence behavior of Ln-POM is usually influenced by the coordination water molecules around Ln^{3+} ions and Ln–O–W bond angles [73]. The strong O–H

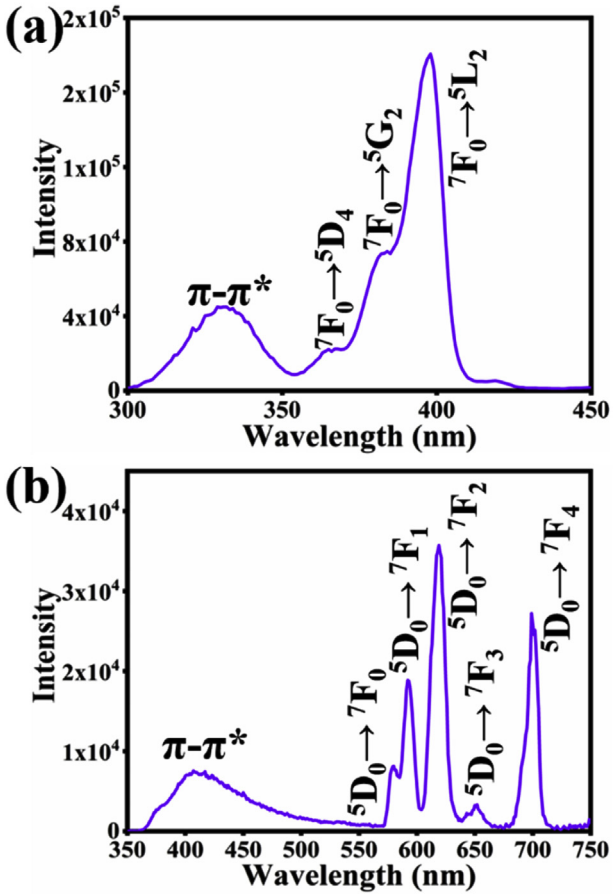

Fig. 4. (a) The photoluminescence excitation spectrum of **1** in aqueous solution under emission at 619 nm; (b) The photoluminescence emission spectrum of **1** in aqueous solution under excitation at 330 nm.

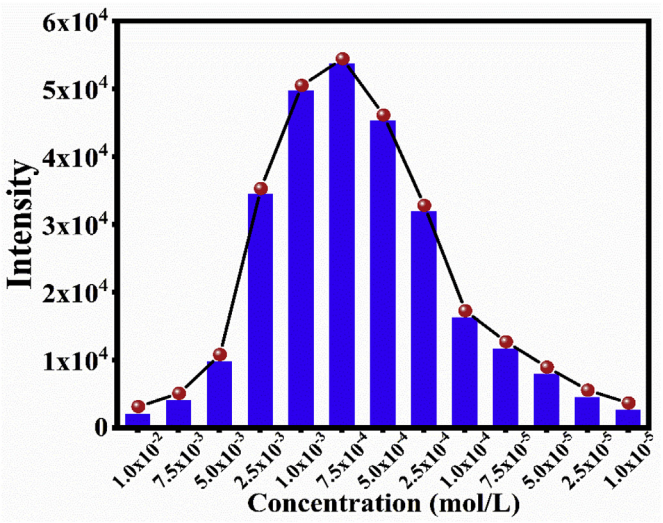

Fig. 5. The changes of histogram and line chart representatives of photoluminescence emission intensity at 619 nm from 1.0×10^{-2} mol/L to 1.0×10^{-5} mol/L concentration gradient of **1** in aqueous solution under excitation at 330 nm.

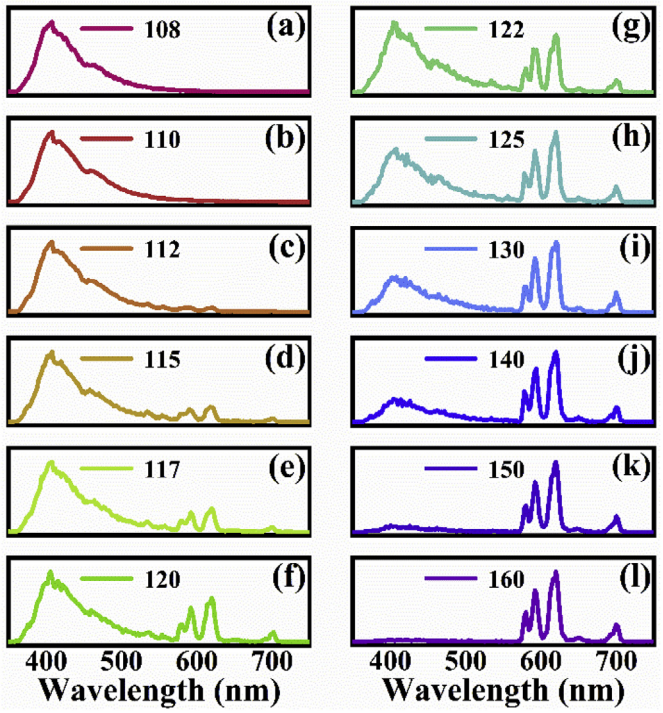

Fig. 6. The microsecond time-resolved emission spectroscopy of **1** in aqueous solution (7.5×10^{-4} mol/L) upon 330 nm excitation (Note that the time-resolved emission spectroscopy from 108 μs to 160 μs).

frequency oscillators of H_2O and other similar coordination molecules will to a great extent quench the luminescence of Ln^{3+} emitting centers. Two water coordination molecules exist around Eu^{3+} ion in **1**, which can affect the emitting emissions of Eu^{3+} ion. Furthermore, the high-efficiency fπ–pπ–dπ orbital mixing will be come true when the Ln–O–W bond angle was about 150°, which also can effectively impair the emission intensity of Ln^{3+} ion. In **1**, the Eu–O–W bond angles of Eu–O30–W1, Eu–O14–W2, Eu–O12–W10 and Eu–O29–W11 were 157.03(19), 136.35(18), 137.54(17) and 156.03(18), respectively, which can not completely lead to luminescent quenching but to some context impede the luminescence of Eu^{3+} center.

Furthermore, the concentration quenching phenomenon usually exists in liquid fluorescence. To testify the phenomenon, a serious of different concentration gradient aqueous solution from 1.0×10^{-2} mol/L to 1.0×10^{-5} mol/L of **1** have been performed at the same conditions (Fig. 5, Fig. S5 and Fig. S6). As shown in Fig. 5, a high concentration solution (1.0×10^{-2} mol/L) of **1** will terribly result in luminescence quenching, and the emission intensity increases to the maximum as the solution concentration decreases until 7.5×10^{-4} mol/L. Subsequently, the emission intensity will decrease with the decreasing of solution concentration of **1** down to 1.0×10^{-5} mol/L, indicating the most optimal emission intensity will come true when the solution concentration was 7.5×10^{-4} mol/L. The decay time curves of **1** at various concentration solution of **1** from 1.0×10^{-2} mol/L to 1.0×10^{-5} mol/L were also performed on the instrument (Fig. S7), and the similar decay profiles indicate the energy transfer dynamics are free from the concentration influence within aqueous solution of **1**, which may be due to aggregation-caused quenching mechanism rather than dynamic collision quenching mechanism.

To elucidate the energy transfer dynamics in **1**, the microsecond time-resolved emission spectroscopy was performed with 330 nm photoexcitation of aqueous solution of **1** (7.5×10^{-4} mol/L) (Fig. 6). An interesting aspect revealed by time-resolved emission spectroscopy is that the distinct layouts evolve within one to second hundreds of microseconds and persist with little change even when the times get delayed from two hundred of microseconds to milliseconds (Fig. S8). After photoexcitation at 330 nm, an intense band around 410 nm was observed at 108 μs (Fig. 6 (a)). Emission observed mainly corresponds to π-π* transition of PHBA molecule, which was well consistent with the

π-π* transition of PHBA ligand in emission spectrum of **1**. In the spectrum at 112 μs (Fig. 6 (c)), the relative weak emissions were found around 592 and 619 nm, which can be assigned to the f-f transitions of Eu^{3+} ion. Subsequently, the emissions at 580, 650 and 700 nm generally were discovered after just 3 μs (Fig. 6 (d)), and the time contact of 3 μs was negligible compared with the longer lifetime of Eu^{3+} emitting center (about 240 μs). As the spectrum decays, the PHBA-centered emission slowly weakens, fade away at 160 μs (Fig. 6 (l)). Meanwhile, the characteristic emissions of Eu^{3+} ion gradually increase (Fig. 6 (d–l)), and the characteristic emission layouts remain little change after 160 μs (Fig. S9). The microsecond time-resolved emission measurements clearly clarified that the sensitization of organic PHBA ligand for Eu^{3+} ion in energy kinetic process after 330 nm photoexcitation of **1** in aqueous solution.

3.6. Sensing properties

According to the photoluminescence study, the aqueous solution of **1** display the considerable emission intensity through sensitization of PHBA group at concentration of 7.5×10^{-4} mol/L, which to some context encourage us to further explore its application in fluorescence detection for sensing metal ions in aqueous solution. To explore the potential of **1** for sensing metal ions in aqueous solution, the photoluminescence spectra of **1** in aqueous solution were recorded with addition of the total fifteen metal ions (Cd^{2+}, Cr^{3+}, Ba^{2+}, K^{+}, Li^{+}, Pb^{2+}, Zn^{2+}, Al^{3+}, Ag^{+}, Hg^{2+}, Co^{2+}, Sr^{2+}, Ca^{2+}, Na^{+}, Mg^{2+}) (Fig. S10). As shown in Fig. 7, the column chart based on emission intensity at 619 nm (**I/I$_0$**, **I** represents the luminescence intensity at 619 nm with addition of metal ions, **I$_0$** represents the initial luminescence intensity at 619 nm without any metal ions) displays the significant differences toward different metal ions. The luminescence with the similar initial intensity were recorded with addition of K^{+}, Li^{+}, Pb^{2+}, Al^{3+}, Hg^{2+}, Sr^{2+}, Na^{+} and Mg^{2+} ions. Interestingly, the luminescence quenching phenomenon were found toward addition of Cr^{3+}, Ag^{+} and Co^{2+} ions, and the luminescence intensity enhanced upon addition of Cd^{2+}, Ba^{2+}, Zn^{2+} and Ca^{2+} ions. In particular, the obvious luminescence quenching and enhanced effects were observed with addition of Cr^{3+} ion and alkaline metal ion Ca^{2+}, respectively.

To carefully explore the sensing properties of **1** for Cr^{3+} ion in aqueous solution, a series of photoluminescence spectra with addition of various concentration of Cr^{3+} ion from 1.0×10^{-6} mol/L to 1.0×10^{-1} mol/L were also recorded at the same condition. As shown in Fig. 8, the luminescence intensity decreases with the increase of

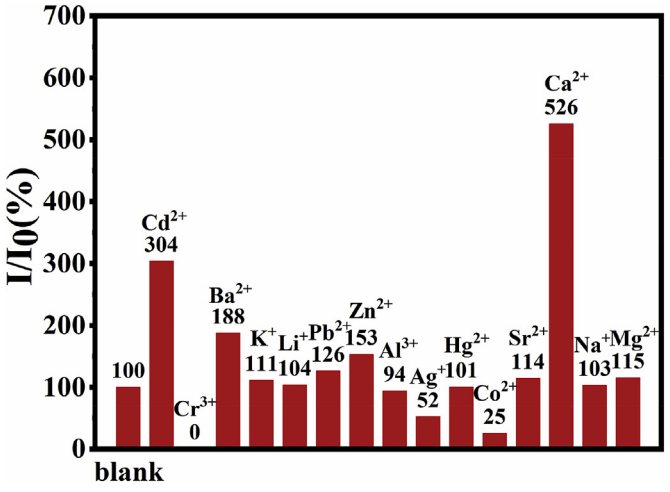

Fig. 7. The changes of luminescence intensity of emission at 619 nm of aqueous solution **1** (7.5×10^{-4} mol/L) with addition of different metal ions. Note that **I** represents the luminescence intensity with addition of metal ions, **I$_0$** represents the initial luminescence intensity (**blank**) without any metal ions.

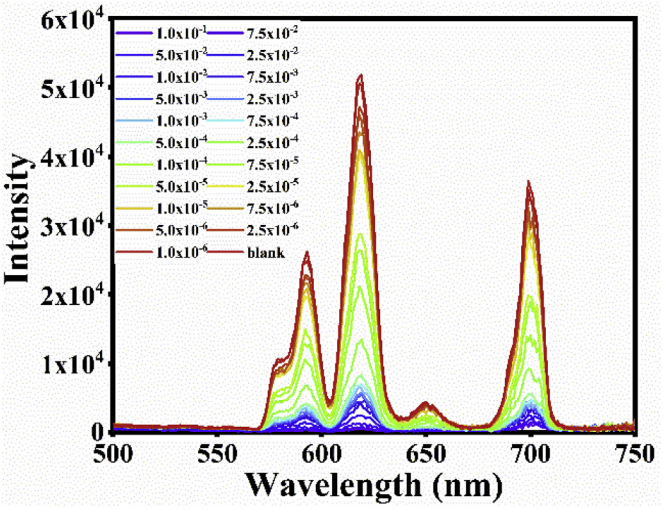

Fig. 8. The emission spectral change of **1** in aqueous solution (7.5×10^{-4} mol/L) with addition of different concentration of Cr^{3+} ion from 1.0×10^{-6} mol/L to 1.0×10^{-1} mol/L.

solution concentration of Cr^{3+} ion, and the intensity was gradually close to the initial luminescence intensity until concentration of Cr^{3+} ion diluted to 1.0×10^{-6} mol/L. The result indicates that **1** can be used for detecting Cr^{3+} ions in aqueous solution through luminescence quenching mechanism. Furthermore, the changes of column representatives of luminescence intensity at 619 nm of an aqueous solution of **1** with addition of different concentration Cr^{3+} ion were carefully manufactured to investigate the relationship between luminescence intensity of **1** and concentration of Cr^{3+} ion (Fig. 9a). Fig. 9b showed that a linear correlation ($R^2 = 0.990$) of the luminescence intensity at 619 nm was seen within the range of 0–10×10^{-6} mol/L with a regression equation of $Y = 51589.913–1131.801X$, from which the detection limit (3σ/k: σ is the standard deviation of blank samples, k is the slope of the linear equation [74,75]) was calculated to be 1.423 μM.

The quenching effect can be also analyzed by the quenching constant based on the luminescence data, which can be calculated by the Stern–Volmer equation [76]:

$$I_0/I = 1 + K_{sv}[M] = 1 + K_q\tau_0[M]$$

Where I_0 and I are the luminescence intensity without and with addition of the quencher. K_q is the quenching rate constant of the Eu^{3+} emitting center, K_{sv} is the dynamic quenching constant, τ_0 is the lifetime of the without quencher and [M] is the concentration of the quencher, respectively. As shown in Table S2, the values of K_q were ranging from 4.34×10^{6} L (mol s)$^{-1}$ to 4.29×10^{9} L (mol s)$^{-1}$, which were all lower than the value of the maximum scatter collision quenching constant (2.0×10^{10} L (mol s)$^{-1}$). Thus, the quenching was more of a dynamic quenching that was initiated by dynamic collision, rather than static quenching by formation of new complexes.

Dynamic and static quenching mechanisms can be also distinguished by changes of the luminescence lifetime. Thus, the luminescence lifetime was also recorded at the same conditions (Fig. 9c). The lifetime decreases with the addition of quenchers for dynamic quenching, while no change is observed for static quenching. Here, the decreasing lifetime for Eu^{3+} emitting center can be clearly confirmed after the addition of increasing concentration of Cr^{3+} ion (Table 1), further indicating the dynamic quenching mechanisms exist between **1** and Cr^{3+} ion in aqueous solution.

In addition, the potential fluorescence sensing ability of **1** for Ca^{2+} ion was also examined with addition of various concentration of Ca^{2+} ion at the same condition. As shown in Fig. 9d and Fig. S11, **1** displays a significant effect on the luminescence intensity after addition of high

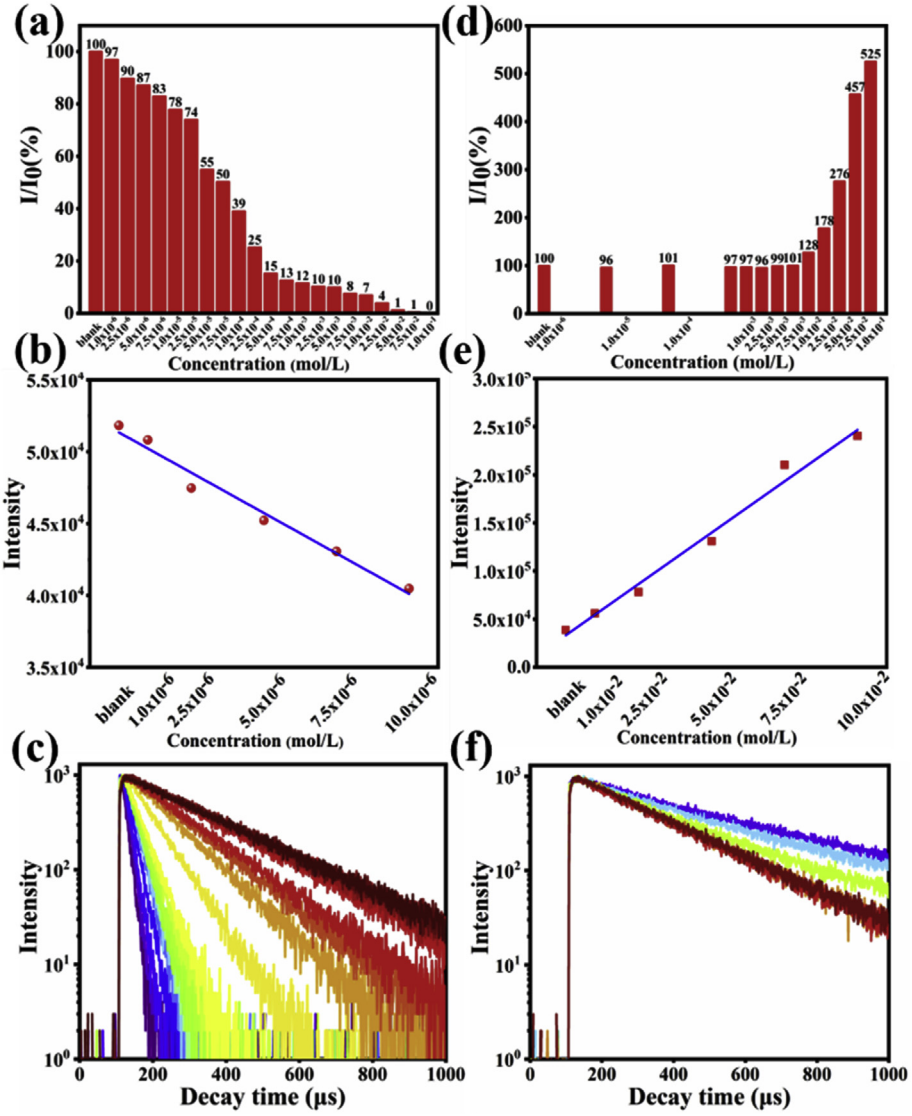

Fig. 9. (a) The changes of column representatives of photoluminescence emission intensity at 619 nm of aqueous solution of **1** (7.5×10^{-4} mol/L) with addition of Cr^{3+} ion from 1.0×10^{-6} mol/L to 1.0×10^{-1} mol/L under 330 nm excitation; **(b)** the liner relationship of photoluminescence emission intensity at 619 nm of aqueous solution of **1** (7.5×10^{-4} mol/L) with addition of Cr^{3+} ion from 1.0×10^{-6} mol/L to 10.0×10^{-6} mol/L under 330 nm excitation; **(c)** The decay time curves of **1** in aqueous solution (7.5×10^{-4} mol/L) detected at 619 nm with addition of Cr^{3+} ion from 1.0×10^{-6} mol/L (red) to 1.0×10^{-1} mol/L (purple) under photoexcitation at 330 nm; **(d)** the changes of column representatives of photoluminescence emission intensity at 619 nm of **1** in aqueous solution (7.5×10^{-4} mol/L) with addition of Ca^{2+} ion from 1.0×10^{-6} mol/L to 1.0×10^{-1} mol/L under 330 nm excitation; **(e)** the liner relationship of photoluminescence emission intensity at 619 nm of aqueous solution of **1** (7.5×10^{-4} mol/L) with addition of Ca^{2+} ion from 1.0×10^{-2} mol/L to 10.0×10^{-2} mol/L under 330 nm excitation; **(f)** The decay time curves of **1** in aqueous solution (7.5×10^{-4} mol/L) detected at 619 nm with addition of Ca^{2+} ion from 1.0×10^{-2} mol/L (red) to 1.0×10^{-1} mol/L (purple) under photoexcitation at 330 nm. Note that **I** represents the luminescence intensity with addition of metal ions, $\mathbf{I_0}$ represents the initial luminescence intensity without any metal ions. (For interpretation of the references to color in this figure legend, the reader is referred to the Web version of this article.)

Table 1
The lifetime changes of **1** under emission at 619 nm with addition of different concentration of Cr^{3+} ion and Ca^{2+} ion.

Ion concentration (mol/L)	Lifetime (μs, Cr^{3+})	Lifetime (μs, Ca^{2+})
blank	240.36	238.90
1.0×10^{-6}	236.43	238.53
2.5×10^{-6}	234.98	
5.0×10^{-6}	229.20	
7.5×10^{-6}	227.27	
1.0×10^{-5}	225.99	237.94
2.5×10^{-5}	213.47	
5.0×10^{-5}	161.23	
7.5×10^{-5}	143.56	
1.0×10^{-4}	117.82	238.73
2.5×10^{-4}	74.80	
5.0×10^{-4}	43.05	
7.5×10^{-4}	38.98	
1.0×10^{-3}	32.88	237.88
2.5×10^{-3}	32.27	238.14
5.0×10^{-3}	31.17	237.32
7.5×10^{-3}	28.94	238.10
1.0×10^{-2}	27.81	239.68
2.5×10^{-2}	23.68	240.73
5.0×10^{-2}	18.38	268.14
7.5×10^{-2}	16.37	322.32
1.0×10^{-1}	13.47	373.68

concentration of Ca^{2+} ion (above 1.0×10^{-2} mol/L). The results indicate that **1** has a selective detection for Ca^{2+} ion with high concentration in aqueous solution. Fig. 9e revealed that a linear correlation ($R^2 = 0.992$) of the luminescence intensity at 619 nm with addition of Ca^{2+} ion from 1.0×10^{-2} mol/L to 10.0×10^{-2} mol/L with a regression equation of $Y = 33696.683 + 2115.021X$, from which the detection limit was calculated to be 0.676 mM. Similarly, the lifetime of **1** were almost unchanged with addition of low concentration Ca^{2+} ion, while the lifetime obviously increased as concentration of Ca^{2+} ion increased (Fig. 9f), indicating a much better energy transfer efficiency from PHBA ligand to Eu^{3+} ion.

3.7. Sensing kinetic study

The existence of Lewis basic oxhydryl active site in this organic-inorganic hybrid structure makes **1** more interesting, which means **1** can be regarded as potential candidate for sensing and detecting metal ions. However, the oxhydryl group may be not always active site for sensing metal ions, due to the relatively weak Lewis basic effect. Herein, two different sensing mechanisms may exist for detecting Cr^{3+} ion and Ca^{2+} ion in aqueous solution, respectively.

As shown in Fig. 10a, both π-π* excitation band intensity of organic PHBA ligand and direct excitation bands intensity of Eu^{3+} ion display a decreasing tendency toward the increasing concentration Cr^{3+} ion,

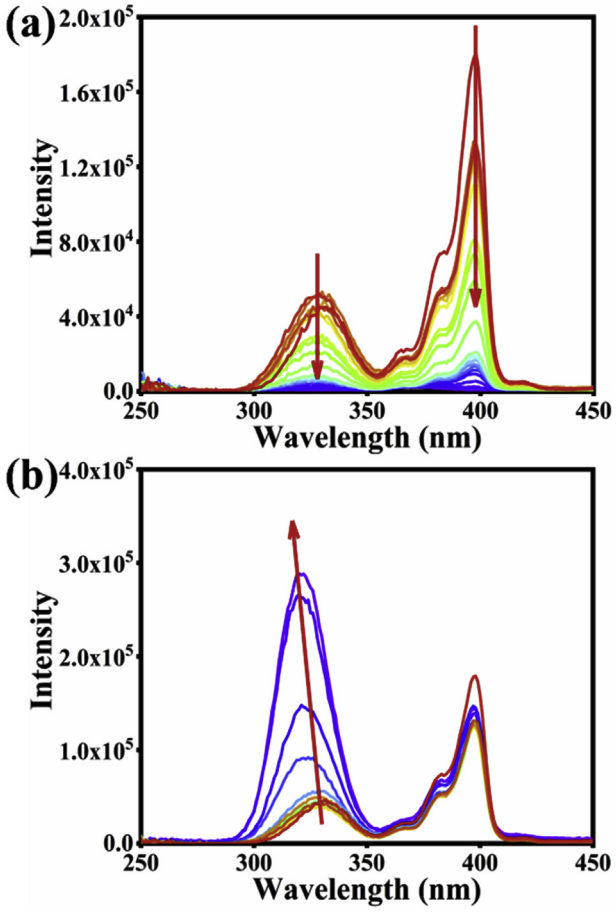

Fig. 10. (a) The excitation spectral change of aqueous solution of **1** (7.5×10^{-4} mol/L) with addition of various concentration of Cr^{3+} ion from 1.0×10^{-6} mol/L (red) to 1.0×10^{-1} mol/L (purple); (b) The excitation spectral change of aqueous solution of **1** (7.5×10^{-4} mol/L) with addition of various concentration of Ca^{2+} ion from 1.0×10^{-6} mol/L (red) to 1.0×10^{-1} mol/L (purple). (For interpretation of the references to color in this figure legend, the reader is referred to the Web version of this article.)

indicating the luminescence quenching active site may be at Eu^{3+} ion rather than the oxhydryl site, which could be explained that the direct f-f excitation intensity of Eu^{3+} ion is rarely influenced if the active site locate at the oxhydryl site of PHBA ligand. Thus, the quenching mechanisms for sensing Cr^{3+} ion can be speculated that mutual collision between Eu^{3+} emitting center and Cr^{3+} ion in aqueous solution cause the produce of a large number of non-radiative transitions, leading to the luminescence quenching phenomenon (Scheme 2a). The violent dynamic collisions can cause the severe luminescence quenching of **1** in aqueous solution with the addition of increasing the concentration of the Cr^{3+} ion.

The sensing mechanism for detecting Ca^{2+} ion can be deemed as the interaction between oxhydryl active site and Eu^{3+} ion. As shown in Fig. 10b, the excitation intensity of π-π* transition of PHBA ligand increase and the band center displays a blue shift phenomenon as the concentration of Ca^{2+} ion increased, while the direct excitation intensity of f-f transitions of Eu^{3+} ion display negligible changes, implying the active site may locate at PHBA ligand rather than Eu^{3+} ion. The effect between Lewis basic oxhydryl active site and Lewis acidic Ca^{2+} ion through electrostatic interaction cause the enhanced energy absorb ability of PHBA ligand, and then transfer more energy to Eu^{3+} ion, leading to a emission enhancement phenomenon (Scheme 2b), which also have been certified by increased lifetime of Eu^{3+} emitting center as the concentration of Ca^{2+} ion increased.

The microsecond time-resolved emission spectroscopy of **1** in aqueous solution with the addition of Cr^{3+} and Ca^{2+} ions were also performed on the instrument at the same conditions (Figs. S11 and S12). The aqueous solution of **1** with addition of Cr^{3+} or Ca^{2+} ions have similar energy transfer dynamics from 108 to 160 μs with that of **1** with addition of no any metal ion; organic PHBA ligand absorb energy and then transfer to sensitize Eu^{3+} ion. However, several differences could be carefully observed during the energy transfer process through the comparisons of transient emission outlays (e.g. 120, 125, 130, 140, 150, 160 μs) (Fig. 11), indicating the different energy transfer efficiency compared to that of the blank. The reason can be explained that **1** interact with Cr^{3+} or Ca^{2+} ions to affect energy transfer efficiency: the dynamic collision between Eu^{3+} ion and Cr^{3+} ion make emitting emissions of Eu^{3+} ions quench and energy transfer weaken from organic PHBA ligand to Eu^{3+} ions; whereas the electrostatic interaction between oxhydryl active site and Ca^{2+} ion facilitate the enhancement

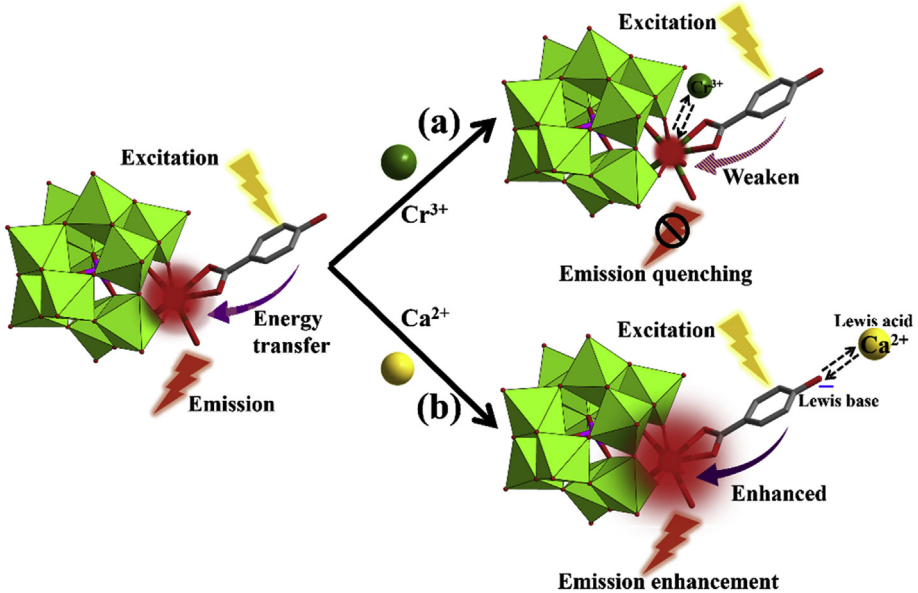

Scheme 2. (a) The illustration of emission quenching mechanism of **1** after addition of Cr^{3+} ion in aqueous solution; (b) The illustration of emission enhancement mechanism of **1** after addition of Ca^{2+} ion in aqueous solution.

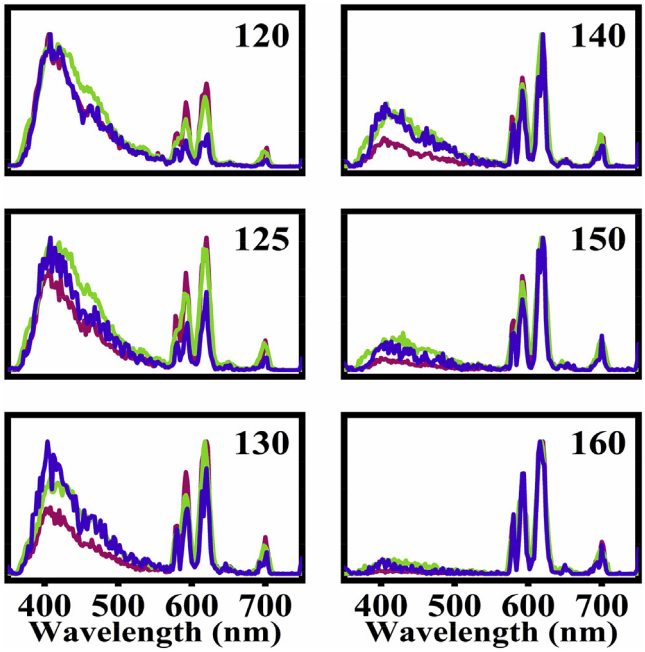

Fig. 11. The comparison of emission spectroscopy of **1** in aqueous solution (pink), the aqueous solution of **1** with addition of Cr^{3+} ion (green), the aqueous solution of **1** with addition of Ca^{2+} ion (purple) at 120, 125, 130, 140, 150 and 160 μs?

of energy absorption of organic PHBA ligand to strengthen emission of Eu^{3+} emitting center. This above hypothesis was also confirmed by the explorations of decay curves: the generally decreased lifetime of **1** in aqueous solution with addition of Cr^{3+} ion at 619 nm was in good agreement with the emission quenching mechanism; the generally increased lifetime of **1** with addition of Ca^{2+} ion at 619 nm was well consist with the energy transfer efficiency enhanced mechanism.

4. Conclusion

In summary, one Eu-POM (**1**) was successfully synthesized using a conventional aqueous method, and the detailed structural analyses of **1** revealed that this Eu-POM possesses a desirable photoluminescence property and can be regarded as a potential fluorescence probe. The photoluminescence properties of **1** in aqueous solution indicate the Eu^{3+} emitting center can be activated by PHBA ligand through energy absorption and then transfer to Eu^{3+} ion, which revealed the Eu-POM analogue can serve as potential probe for the recognition of metal ions in aqueous solution. The results of detection for sensing several metal ions in aqueous solution reveal **1** not only detect Cr^{3+} ion through luminescence quenching mechanism, but also probe Ca^{2+} ion through luminescence enhancement mechanism. The detection limits for detecting Cr^{3+} and Ca^{2+} ion were 1.423 μM and 0.676 mM, respectively. The exploration of luminescence quenching and enhancement mechanisms manifest that violent dynamic collisions between Eu^{3+} ion and Cr^{3+} ion cause the severe luminescence quenching and electrostatic interaction between Lewis basic oxhydryl active site and Lewis acidic Ca^{2+} ion leads to a luminescence enhancement phenomenon of **1** in aqueous solution. Considering that this thinking may to some extent broaden the potential application of Ln-POM derivatives as luminescence probes, the following works will continue to look forward to synthesizing and exploring novel and useful resulting Ln-POMs.

Acknowledgments

This work was financially supported by the National Natural Science Foundation of China of China (21771053, 21771054, 21571050 and 21573056), Natural Science Foundation of Henan Province (132300410144 and 162300410015), Henan Province Science and Technology Attack Plan Project (182102210237) and the 2019 Students Innovative Pilot Plan of Henan University (201910475076).

Appendix A. Supplementary data

Supplementary data to this article can be found online at https://doi.org/10.1016/j.dyepig.2019.107696.

Conflicts of interest

The authors declare that they have no conflict of interest.

References

[1] Gaeta A, Hider RC. The crucial role of metal ions in neurodegeneration: the basis for a promising therapeutic strategy. Br J Pharmacol 2005;146:1041–59.
[2] Yang Z, Loh KY, Chu YT, Feng R, Satyavolu NSR, Xiong M, Nakamata Huynh SM, Hwang K, Li L, Xing H, Zhang X, Chemla YR, Gruebele M, Lu Y. Optical control of metal ion probes in cells and zebrafish using highly selective DNAzymes conjugated to upconversion nanoparticles. J Am Chem Soc 2018;140:17656–65.
[3] Nolan EM, Lippard SJ. A "turn-on" fluorescent sensor for the selective detection of mercuric ion in aqueous media. J Am Chem Soc 2003;125:14270–1.
[4] Ji G, Liu J, Gao X, Sun W, Wang J, Zhao S, Liu Z. A luminescent lanthanide MOF for selectively and ultra-high sensitively detecting Pb^{2+} ions in aqueous solution. J Mater Chem A 2017;5:10200–5.
[5] Li L, Chen Q, Niu Z, Zhou X, Yang T, Huang W. Lanthanide metal–organic frameworks assembled from a fluorene-based ligand: selective sensing of Pb^{2+} and Fe^{3+} ions. J Mater Chem C 2016;4:1900–5.
[6] Paul S, Manna A, Goswami S. A differentially selective molecular probe for detection of trivalent ions (Al^{3+} , Cr^{3+} and Fe^{3+}) upon single excitation in mixed aqueous medium. Dalton Trans 2015;44:11805–10.
[7] Zhang H, Sun T, Ruan Q, Zhao J, Mu L, Zeng X, Jin Z, Su S, Luo Q, Yan Y, Redshaw C. A multifunctional tripodal fluorescent probe for the recognition of Cr^{3+}, Al^{3+}, Zn^{2+} and F^- with controllable ESIPT processes. Dyes Pigments 2019;162:257–65.
[8] Faraz M, Abbasi A, Naqvi FK, Khare N, Prasad R, Barman I, Pandey R. Polyindole/cadmium sulphide nanocomposite based turn-on, multi-ion fluorescence sensor for detection of Cr^{3+}, Fe^{3+} and Sn^{2+} ions. Sens Actuators B 2018;269:195–202.
[9] Zhou Y, Zhang J, Zhang L, Zhang Q, Ma T, Niu J. A rhodamine-based fluorescent enhancement chemosensor for the detection of Cr^{3+} in aqueous media. Dyes Pigments 2013;97:148–54.
[10] Fu HR, Wang N, Qin JH, Han ML, Ma LF, Wang F. Spatial confinement of a cationic MOF: a SC-|SC approach for high capacity Cr(VI)-oxyanion capture in aqueous solution. Chem Commun 2018;54:11645–8.
[11] Dong C, Wu G, Wang Z, Ren W, Zhang Y, Shen Z, Li T, Wu A. Selective colorimetric detection of Cr(III) and Cr(VI) using gallic acid capped gold nanoparticles. Dalton Trans 2016;45:8347–54.
[12] Puthiyedath T, Bahulayan D. A click derived triazole-coumarin derivative as fluorescence on-off PET based sensor for Ca^{2+} and Fe^{3+} ions. Sens Actuators B 2018;272:110–7.
[13] Lin Y, Zheng Y, Guo Y, Yang Y, Li H, Fang Y, Wang C. Peptide-functionalized carbon dots for sensitive and selective Ca^{2+} detection. Sens Actuators B 2018;273:1654–9.
[14] Owlad M, Aroua MK, Ashri WDW, Baroutian S. Removal of hexavalent chromium-contaminated water and wastewater: a review. Water, Air, Soil Pollut 2009;200:59–77.
[15] Gode F, Pehlivan E. Removal of Cr(VI) from aqueous solution by two Lewatit-anion exchange resins. J Hazard Mater 2005;119:175–82.
[16] Yang XG, Ma LF, Yan DP. Facile synthesis of 1D organic–inorganic perovskite micro-belts with high water stability for sensing and photonic applications. Chem Sci 2019;10:4567–72.
[17] Wang H, Kim Y, Liu H, Zhu Z, Bamrungsap S, Tan W. Engineering a unimolecular DNA-catalytic probe for single lead ion monitoring. J Am Chem Soc 2009;131:8221–6.
[18] Kimura E, Koike T. Recent development of zinc-fluorophores. Chem Soc Rev 1998;27:179–84.
[19] Nolan EM, Lippard SJ. Small-molecule fluorescent sensors for investigating zinc metalloneurochemistry. Acc Chem Res 2009;42:193–203.
[20] Salinas Y, Martínezmáñez R, Marcos MD, Sancenón F, Costero AM, Parra M, Gil S. Optical chemosensors and reagents to detect explosives. Chem Soc Rev 2012;41:1261–96.
[21] Hu Z, Deibert BJ, Li J. Luminescent metal-organic frameworks for chemical sensing and explosive detection. Chem Soc Rev 2014;43:5815–40.
[22] Thomas SW, Joly GD, Swager TM. Chemical sensors based on amplifying fluorescent conjugated polymers. Chem Rev 2007;107:1339–86.
[23] Xiang Z, Fang C, Leng S, Cao D. An amino group functionalized metal–organic framework as a luminescent probe for highly selective sensing of Fe^{3+} ions. J Mater Chem A 2014;2:7662–5.
[24] Min Z, Tan H, Xie Z, Zhang L, Jing X, Sun Z. Fast response and high sensitivity Europium metal organic framework fluorescent probe with chelating terpyridine sites for Fe^{3+}. ACS Appl Mater Interfaces 2013;5:1078–83.

[25] Jayaramulu K, Narayanan RP, George SJ, Maji TK. Luminescent microporous metal-organic framework with functional Lewis basic sites on the pore surface: specific sensing and removal of metal ions. Inorg Chem 2012;51:10089–91.

[26] Jiang S, Uch B, Agarwal S, Greiner A. Ultralight, thermally insulating, compressible polyimide fiber assembled sponges. ACS Appl Mater Interfaces 2017;9:32308–15.

[27] Ding Q, Xu X, Yue Y, Mei C, Huang C, Jiang S, Wu Q, Han J. Nanocellulose-mediated electroconductive self-healing hydrogels with high strength, plasticity, viscoelasticity, stretchability, and biocompatibility toward multifunctional applications. ACS Appl Mater Interfaces 2018;10:27987–8002.

[28] Lv D, Wang R, Tang G, Mou Z, Lei J, Han J, Smedt S, Xiong R, Huang C. Ecofriendly electrospun membranes loaded with visible-light-responding nanoparticles for multifunctional usages: highly efficient air filtration, dye scavenging, and bactericidal activity. ACS Appl Mater Interfaces 2019;11:12880–9.

[29] Wu D, Chen L, Lee W, Ko G, Yin J, Yoon J. Recent progress in the development of organic dye based near-infrared fluorescence probes for metal ions. Coord Chem Rev 2018;354:74–97.

[30] Gao S, Tang G, Hua D, Xiong R, Han J, Jiang S, Zhang Q, Huang C. Stimuli-responsive bio-based polymeric systems and their applications. J Mater Chem B 2019;7:709–29.

[31] Ma P, Hu F, Wang J, Niu J. Carboxylate covalently modified polyoxometalates: from synthesis, structural diversity to applications. Coord Chem Rev 2019;378:281–309.

[32] Song YF, Tsunashima R. Recent advances on polyoxometalate-based molecular and composite materials. Chem Soc Rev 2012;41:7384–402.

[33] Wu H, Zhi M, Chen H, Singh V, Ma P, Wang J, Niu J. Well-tuned white-light-emitting behaviours in multicenter-Ln polyoxometalate derivatives: a photoluminescence property and energy transfer pathway study. Spectrochim. Acta A Mol. Biomol. Spectrosc. 5 December 2019;223https://doi.org/10.1016/j.saa.2019.117294.

[34] Wu H, Ma T, Wu C, Yan L, Su Z. Effect of polyoxometalate in organic-inorganic hybrids on charge transfer and absorption spectra towards sensitizers. Dyes Pigments 2017;142:379–86.

[35] Wu D, Chen W, Wang T, Li F, Li J, Wang E. Synthesis of copper(II)–imidazole complex modified sandwich-type polyoxometalates for enhancing the power conversion efficiency in dye-sensitized solar cells. Dyes Pigments 2019;168:151–9.

[36] Liu J, Han Q, Chen L, Zhao J. A brief review of the crucial progress on heterometallic polyoxotungstates in the past decade. CrystEngComm 2016;18:842–62.

[37] Oms O, Dolbecq A, Mialane P. Diversity in structures and properties of 3d-incorporating polyoxotungstates. Chem Soc Rev 2012;41:7497–536.

[38] Zhao JW, Li YZ, Chen LJ, Yang GY. Research progress on polyoxometalate-based transition-metal–rare-Earth heterometallic derived materials: synthetic strategies, structural overview and functional applications. Chem Commun 2016;52:4418–45.

[39] Wu H, Wan R, Si Y, Ma P, Wang J, Niu J. A helical chain-like organic-inorganic hybrid arsenotungstate with color-tunable photoluminescence. Dalton Trans 2018;47:1958–65.

[40] Wu H, Meng X, Wan R, Ma P, Wang J, Niu J. A new dimeric polyoxometalate derivate assembled by divacant Dawson $\{P_2W_{16}\}$ units and isosceles triangle $\{Ce_3\}$ cluster. Inorg Chem Commun 2018;95:154–7.

[41] Zhang C, Howell RC, McGregor D, Bensaid L, Rahyab S, Nayshtut M, Lekperic S, Francesconi LC. Synthesis of a cluster containing Eu(III) α_2-$P_2W_{17}O_{61}^{10-}$ and preliminary luminescence experiments. Compt Rendus Chem 2005;8:1035–44.

[42] Wu H, Yan B, Li H, Singh V, Ma P, Wang J, Niu J. Enhanced photostability luminescent properties of Er^{3+}-doped near-white-emitting $Dy_xEr_{(1-x)}$-POM derivatives. Inorg Chem 2018;57:7665–75.

[43] Kaczmarek AM, Liu J, Laforce B, Vincze L, Van HK, Van DR. Cryogenic luminescent thermometers based on multinuclear Eu^{3+}/Tb^{3+} mixed lanthanide polyoxometalates. Dalton Trans 2017;46:5781–5.

[44] Hungerford G, Suhling K, Green M. Luminescence enhancement of a europium containing polyoxometalate on interaction with bovine serum albumin. Photochem Photobiol Sci 2008;7:734–7.

[45] Zheng L, Ma Y, Zhang G, Yao J, Keita B, Nadjo L. A multitechnique study of europium decatungstate and human serum albumin molecular interaction. Phys Chem Chem Phys 2010;12:1299–304.

[46] Zhang H, Guo LY, Xie Z, Xin X, Sun D, Yuan S. Tunable aggregation-induced emission of polyoxometalates via amino acid-directed self-assembly and their application in detecting dopamine. Langmuir 2016;32:13736–45.

[47] Yang J, Chen M, Li P, Cheng F, Xu Y, Li Z, Wang Y, Li H. Self-healing hydrogel containing Eu-polyoxometalate as acid-base vapor modulated luminescent switch. Sens Actuators B 2018;273:153–8.

[48] Salomon W, Dolbecq A, Roch-Marchal C, Paille G, Dessapt R, Mialane P, Serier-Brault H. A multifunctional dual-luminescent polyoxometalate@metal-organic framework EuW10@UiO-67 composite as chemical probe and temperature sensor. Frontiers in Chemistry 2018;6:425.

[49] Tian A, Yang M, Fu Y, Ying J, Wang X. Electrocatalytic and Hg^{2+} fluorescence identifiable bifunctional sensors for a series of Keggin compounds. Inorg Chem 2019;58:4190–200.

[50] Ji H, Li X, Xu D, Zhou Y, Zhang L, Zuhra Z, Yang S. Synthesis, structure, and photoluminescence of color-tunableand white-light-emitting lanthanide metal-organic open frameworks composed of $AlMo_6(OH)_6O_{18}^{3-}$ polyanion and nicotinate. Inorg Chem 2017;56:156–66.

[51] Ritchie C, Moore EG, Speldrich M, Kögerler P, Boskovic C. Terbium polyoxometalate organic complexes: correlation of structure with luminescence properties. Angew Chem, Int Ed 2010;49:7702–5.

[52] Zhao B, Chen XY, Cheng P, Liao DZ, Shiping Yan A, Jiang ZH. Coordination polymers containing 1D channels as selective luminescent probes. J Am Chem Soc 2004;126:15394–5.

[53] Liu W, Jiao T, Li Y, Liu Q, Tan M, Wang H, Wang L. Lanthanide coordination polymers and their Ag^+-modulated fluorescence. J Am Chem Soc 2004;126:2280–1.

[54] Hao Z, Song X, Min Z, Xing M, Zhao S, Su S, Zhang H. One-dimensional channel-structured Eu-MOF for sensing small organic molecules and Cu^{2+} ion. J Mater Chem A 2013;1:11043–50.

[55] Sharif T, Niaz A, Najeeb M, Zaman MI, Ihsan M. Sirajuddin, Isonicotinic acid hydrazide-based silver nanoparticles as simple colorimetric sensor for the detection of Cr^{3+}. Sens Actuators B 2015;216:402–8.

[56] Saha S, Mahato P, Upendar RG, Suresh E, Chakrabarty A, Baidya M, Ghosh SK, Das A. Recognition of Hg^{2+} and Cr^{3+} in physiological conditions by a rhodamine derivative and its application as a reagent for cell-imaging studies. Inorg Chem 2012;51:336–45.

[57] Gupta VK, Jain AK, Kumar P, Agarwal S, Maheshwari G. Chromium(III)-selective sensor based on tri-o-thymotide in PVC matrix. Sensor Actuator B Chem 2006;113:182–6.

[58] Tourne CM, Tourne GF. Aquanonadecatungstodiphosphate(14–) polyanion, $[P_2W_{19}O_{69}(OH_2)]^{14-}$: X-ray crystallographic structure of its potassium salt, chemical relationships in the tungstophosphate system, and conversion into the diaquaicosatungstodiphosphate $[P_2W_{20}O_{70}(OH_2)_2]^{10-}$. J Chem Soc, Dalton Trans 1988:2411–20.

[59] Li HL, Liu YJ, Liu JL, Chen LJ, Zhao JW, Yang GY. Structural transformation from dimerization to tetramerization of serine-decorated rare-earth-incorporated arsenotungstates induced by the usage of rare-earth salts. Chem - Eur J 2017;23:2673–89.

[60] Sheldrick GM. Crystal structure refinement with SHELXL. Acta Crystallogr C: Struct Chem 2015;C71:3–8.

[61] Spek AL. PLATON SQUEEZE: a tool for the calculation of the disordered solvent contribution to the calculated structure factors. Acta Crystallogr C: Struct Chem 2015;C71:9–18.

[62] Yang H, Liu S, Cao L, Jiang S, Hou H. Superlithiation of non-conductive polyimide toward high-performance lithium-ion batteries. J Mater Chem A 2018;6:21216–24.

[63] Lv D, Zhu M, Jiang Z, Jiang S, Zhang Q, Xiong R, Huang C. Green electrospun nanofbers and their application in air filtration. Macromol Mater Eng 2018;303:1800336.

[64] Parbhakar S, Kaushik R, Hussain F. Synthesis and characterization of self-assembled inorganic-organic hybrid arsenotungstates. Acta Crystallogr C: Struct Chem 2018;C74:1561–8.

[65] Zhang C, Zhang M, Shi H, Zeng Q, Zhang D, Zhao Y, Wang Y, Ma P, Wang J, Niu J. A high-nuclearity isopolyoxotungstate based manganese cluster: one-pot synthesis and step-by-step assembly. Chem Commun 2018;54:5458–61.

[66] Yamase T. Chapter 243 luminescence of polyoxometallolanthanoates and photochemical nano-ring formation. Handbook on the physics and chemistry of rare earths, vol. 39. Elsevier; 2009. p. 297–356.

[67] Yamase T. Photo- and electrochromism of polyoxometalates and related materials. Chem Rev 1998;98:307–25.

[68] Ritchie C, Baslon V, Moore EG, Reber C, Boskovic C. Sensitization of lanthanoid luminescence by organic and inorganic ligands in lanthanoid-organic-polyoxometalates. Inorg Chem 2012;51:1142–51.

[69] Ma P, Hu F, Wan R, Huo Y, Zhang D, Niu J, Wang J. Magnetic double-tartaric bridging mono-lanthanide substituted phosphotungstates with photochromic and switchable luminescence properties. J Mater Chem C 2016;4:5424–33.

[70] Chen S, Ma P, Luo H, Wang Y, Niu J, Wang J. A luminescent polyoxoniobate lanthanide derivative $\{Eu_3(H_2O)_9[Nb_{48}O_{138}(H_2O)_6]\}^{27-}$. Chem Commun 2017;53:3709–12.

[71] Ma P, Hu F, Huo Y, Zhang D, Zhang C, Niu J, Wang J. Magnetoluminescent bifunctional dysprosium-based phosphotung-states with synthesis and correlations between structures and properties. Cryst Growth Des 2017;17:1947–56.

[72] Wu H, Zhi M, Singh V, Li H, Ma P, Wang J, Niu J. Elucidating white light emissions in Tm^{3+}/Dy^{3+} codoped polyoxometalates: a color tuning and energy transfer mechanism study. Dalton Trans 2018;47:13949–56.

[73] Artetxe B, Reinoso S, San Felices L, Lezama L, Gutierrez-Zorrilla JM, García JA, Galan-Mascaros JR, Haider A, Kortz U, Vicent C. Cation-directed dimeric versus tetrameric assemblies of lanthanide-stabilized dilacunary Keggin tungstogermanates. Chem - Eur J 2014;20:12144–56.

[74] Song H, Zhang J, Wang X, Zhou Y, Xu C, Pang X, Peng X. A novel “turn-on” fluorescent probe with a large Stokes shift for homocysteine and cysteine: performance in living cells and zebrafish. Sensor Actuator B Chem 2018;259:233–40.

[75] Jiang K, Chen S, Luo S, Pang C, Wu X, Wang Z. Concise design and synthesis of water-soluble fluorescence sensor for sequential detection of Zn(II) and picric acid via cascade mechanism. Dyes Pigments 2019;167:164–73.

[76] Zhang ZM, Duan X, Yao S, Wang Z, Lin Z, Li YG, Long LS, Wang EB, Lin W. Cation-mediated optical resolution and anticancer activity of chiral polyoxometalates built from entirely achiral building blocks. Chem Sci 2016;7:4220–9.